Scientific Research Publishing

Open Journal of Applied Sciences, 2026, 16(1), 115-142
https://www.scirp.org/journal/ojapps
ISSN Online: 2165-3925
ISSN Print: 2165-3917

Simulation Study of the Consequences of Electromagnetic Waves on High-Voltage AC Power Transmissin Lines Using Numerical Methods

Anthony Bassesuka Sandoka Nzao[1*], Moengo Hahe Christian[2]

[1]ISTA Kinshasa, Electrical Engineering, Kinshasa, Democratic Republic of Congo
[2]ISTA Kinshasa Doctoral School, Electrical Engineering, Kinshasa, Democratic Republic of Congo
Email: *bass_sandoka@yahoo.fr

How to cite this paper: Nzao, A.B.S. and Christian, M.H. (2026) Simulation Study of the Consequences of Electromagnetic Waves on High-Voltage AC Power Transmissin Lines Using Numerical Methods. *Open Journal of Applied Sciences*, **16**, 115-142.
https://doi.org/10.4236/ojapps.2026.161009

Received: November 22, 2025
Accepted: January 5, 2026
Published: January 8, 2026

Abstract

When alternating current power transmission lines exceed a certain length, the electrical parameters become highly dependent on distance and frequency. Under these conditions, the lines behave like electromagnetic waveguides, generating significant capacitive and inductive effects. The propagation of these waves leads to phenomena such as no-load overvoltages Ferranti effect, reactive power losses, harmonic currents in the neutral conductor, transformer saturation, and nuisance tripping of protection systems. These disturbances can also affect electronic control circuits and, to a lesser extent, pose health risks to workers exposed to intense electromagnetic fields, this aspect is considered outside the scope of the analysis of this article. Controlling these phenomena is crucial for maintaining the quality and stability of the transmitted power, which poses a significant challenge for modern electrical grids. The objective of this work is to simulate and study the consequences of electromagnetic wave propagation in a long-distance, high-voltage alternating current transmission line and to propose strategies for reducing no-load overvoltages. To this end, two complementary approaches are investigated, an analytical approach based on classical telegraph equations, derived from Maxwell's equations, and a numerical approach based on the FDTD method, widely used to solve nonlinear transient phenomena. The long-distance, high-voltage AC transmission line was modelled by an equivalent passive two-port network, while Kirchhoff's laws and Ohm's law were used to optimise the representation of disturbances. The distributed insertion of series capacitors and shunt inductors was also studied as a solution for reducing capacitive current. The two-dimensional simulations performed show that the analytical and numer-

ical approaches used provide consistent and satisfactory results, allowing for a better understanding and prediction of the occurrence of overvoltages over long distances.

Keywords

Electromagnetic Waves, High-Voltage Line, Alternating Current, Maxwell's Equations, FDTD Method, Modeling, 2D Simulation, Ferranti Effect, Electric and Magnetic Fields, Capacitive and Inductive Effects

1. Introduction

Electrical energy is a key driver of economic and social development, as it is generated, transmitted, and distributed to consumption centres via complex networks [1]-[3]. In most countries, high-voltage power is transmitted using alternating current (AC), although high-voltage direct current (HVDC) lines are experiencing significant growth due to their low losses over very long distances [4]-[7]. Overhead high-voltage lines are generally made of aluminium alloy conductors supported by pylons or poles made of steel, concrete, or composite materials [8]-[10].

They are subject to the same constraints as conventional lines, including thermal limits, voltage drop, voltage stability, and the management of active and reactive power [11]-[13]. Since the 1960s, some lines have been operated at voltages above 765 kV, which has significantly increased their transmission capacity [14]-[16]. Although HVDC systems reduce line losses, their use is sometimes limited by the absence of DC transformers and the complexity of converter stations [17]-[18]. In contrast, HVDC lines remain widely used due to their flexibility, voltage transformation capacity, and compatibility with existing infrastructure [18]-[20].

However, when the length of a line exceeds a certain threshold ($l > 250$ km), electromagnetic phenomena become predominant: electrical quantities are highly dependent on distance and frequency, making purely analytical approaches difficult [21] [22]. Long lines then behave like distributed structures where significant capacitive and inductive effects appear, which can cause no-load overvoltages (or the Ferranti effect), reactive power losses, harmonic currents in the neutral, transformer saturation, and nuisance protection tripping [23]-[25]. These disturbances can affect network performance, cause dangerous transients, and disrupt sensitive electronic circuits [26] [27].

In this context, understanding and modeling electromagnetic phenomena in long-distance high-voltage AC transmission lines is crucial for the stability of modern networks. Analytical methods based on telegraph equations are effective for lines of moderate length but become difficult to apply when wave propagation must be taken into account [28]. Conversely, numerical methods such as Finite-Difference Time-Domain (FDTD) allow for the solution of Maxwell's equations in complex transient regimes, including for very long lines.

This article addresses this issue and aims to study, through simulation, the effects of electromagnetic waves in a long-distance high-voltage AC transmission line. Two complementary approaches are used:

1) The analytical approach, based on telegraph equations and the equivalent two-port network model;

2) A numerical approach, based on the FDTD method, is used to solve Maxwell's equations in the time domain.

Furthermore, solutions such as the distributed addition of series capacitors and shunt inductors are analysed to reduce no-load overvoltages and optimise the quality of the transmitted power. The resulting 2D simulations demonstrate that the models and tools used allow for the accurate evaluation of the phenomena under study and guide technical choices regarding disturbance mitigation.

2. Methods

A simulation study of the consequences of electromagnetic waves on a long-distance AC power transmission line can be carried out using several methods. This article explores two methods, analytical and numerical. The first method relies on Maxwell's equations, which study electromagnetic fields and their interactions [21]-[23]. In their differential form, these equations describe the sources (charges and currents) and the evolution of the electric ($\boldsymbol{E}$) and magnetic ($\boldsymbol{B}$) fields [24]-[27]. The second method relies on telegraph equations, solved using the FDTD method, to predict this phenomenon. The passive two-port network model was chosen and used to model the long-distance EHV line. Kirchhoff's laws and Ohm's law were also used to optimise these disturbances. Appropriately distributed series capacitors and shunt inductors can be used along the EHV line to reduce the capacitive current.

2.1. Modeling of the High Voltage Power Line

Power line modeling allows us to represent their expected electrical behaviour. The main modeling method is based on a system of two partial differential equations that describe the evolution of voltage and current on a power line as a function of distance and time. Two methods, with completely distinct foundations, are used:

- Field theory, developed from Maxwell's equations [23], is rigorous but not always easy to apply and allows us to establish the second theory (circuit theory).
- Circuit theory: modeling propagation along the line by constructing an equivalent circuit (inductors, capacitors, resistors), the analysis of which is simple.

In this article, we will limit ourselves to field theory. Indeed, field theory, developed from Maxwell's equations [27], is rigorous but not always easy to apply and allows us to establish the second theory (circuit theory). At any point in space, which is not located on a surface separating two media, that is, in a linear, homogeneous, and isotropic (LHI) medium, Maxwell's general equations specify that [28]:

$$\nabla \times \boldsymbol{E}(t,r) = -\frac{\partial \boldsymbol{B}(t,r)}{\partial t} \tag{1}$$

$$\nabla \times \boldsymbol{H}(t,r) = \boldsymbol{J}(t,r) + \varepsilon_0 \frac{\partial \boldsymbol{E}(t,r)}{\partial t} \tag{2}$$

$$\nabla \cdot \boldsymbol{D}(t,r) = \rho(t,r) \tag{3}$$

$$\nabla \cdot \boldsymbol{B}(t,r) = 0 \tag{4}$$

The basic variables of these equations are:

$\boldsymbol{B}$: Magnetic induction (T);

$\boldsymbol{H}$: Magnetic field strength (A/m);

$\boldsymbol{D}$: Electric flux density (C/m^2);

$\boldsymbol{E}$: Electric field density (V/m);

$\boldsymbol{J}$: Electric current density (A/m^2);

ρ : Electric charge density (C/m^3).

With:

$$B = \mu \boldsymbol{H} \tag{5}$$

$$\boldsymbol{D} = \varepsilon \boldsymbol{E} \tag{6}$$

$$\boldsymbol{J} = \sigma \boldsymbol{E} \tag{7}$$

and:

μ : Magnetic permeability in Tm^2/A;

ε : Electrical permeability in Cm^{-3}/V;

σ : Electrical conductivity.

In this form, called local or differential, Maxwell's equations express relationships between spatial variations of certain fields and temporal variations of other fields [26] [27].

In a vacuum:

$$\boldsymbol{B}(t,r) = \mu_0 \boldsymbol{H}(t,r) \tag{8}$$

$$\boldsymbol{D}(t,r) = \varepsilon_0 \boldsymbol{E}(t,r) \tag{9}$$

Then Maxwell's equations become [26] [27]:

$$\nabla \times \boldsymbol{H}(t,r) = \varepsilon_0 \frac{\partial \boldsymbol{E}(t,r)}{\partial t} \tag{10}$$

$$\nabla \cdot \boldsymbol{H}(t,r) = 0 \tag{11}$$

$$\nabla \cdot \boldsymbol{B}(t,r) = 0 \tag{12}$$

The differential operator nabla ¨ ∇ ¨ is used to express the curl operation $\nabla \times = \text{rot}$ and the divergence operation $\nabla \cdot = \text{div}$. Maxwell's equations can also be expressed in "global form" as follows [26] [27]:

$$\oint_c \boldsymbol{E}(t,r)\,\mathrm{d}\boldsymbol{l} = -\int_s \boldsymbol{n} \frac{\partial \boldsymbol{B}(t,r)}{\partial t}\,\mathrm{d}A \tag{13}$$

$$\oint_c \boldsymbol{H}(t,r)\mathrm{d}\boldsymbol{l} = -\int_s \boldsymbol{n}\left(\frac{\partial \boldsymbol{D}(t,r)}{\partial t} + \boldsymbol{J}(t,r)\right)\mathrm{d}A \tag{14}$$

After integrating Equations (13) and (14), using the divergence theorem, the two Equations (4) and (6) then become [26] [27]:

$$\oint_c \boldsymbol{n}\boldsymbol{D}(t,r)\mathrm{d}A = \int_v \rho(t,r)\mathrm{d}A \tag{15}$$

$$\int_s \boldsymbol{n}\boldsymbol{B}(t,r)\mathrm{d}A = 0 \tag{16}$$

The boundary conditions for the fields are [26] [27]:

$$\boldsymbol{n}\times\left[\boldsymbol{E}_1(t,r) - \boldsymbol{E}_1(t,r)\right] = 0 \tag{17}$$

$$\boldsymbol{n}\times\left[\boldsymbol{H}_1(t,r) - \boldsymbol{H}_2(t,r)\right] = \boldsymbol{j}_S \tag{18}$$

$$\boldsymbol{n}\times\left[\boldsymbol{D}_1(t,r) - \boldsymbol{D}_2(t,r)\right] = \rho_S \tag{19}$$

$$\boldsymbol{n}\times\left[\boldsymbol{B}_1(t,r) - \boldsymbol{B}_2(t,r)\right] = 0 \tag{20}$$

or:

$\boldsymbol{n}$: is the normal to the separation surface, going from medium 2 to medium 1;

$\boldsymbol{j}_S$: is the surface current density in (A/m^2);

ρ_S: is the surface charge density in (C/m^2).

Modeling of High-Voltage AC Power Lines

The π modeling of power lines (see Figure 1 below) allows us to represent their expected electrical behaviour. It is based on telegraphers' equations [28]-[30]. This model provides accurate results within a certain range of assumptions corresponding to its use; these are black boxes (four-pole models) for which the notion of representing the physical reality of the phenomena disappears, and only the data-results relationship matters. Models used for the design and operation of networks fall into this category. Their limited use leads to simpler models requiring less computing power. Consequently, they are more easily integrated into large simulation suites that allow us to discover a wide range of phenomena [31].

A portion of a power line can be represented by the four-terminal network in Figure 2 below, where [31]-[35]:

• The linear resistance (per unit length) R of the conductor is represented by a series resistance (expressed in ohms per unit length).

- The linear inductance L is represented by an inductance (Henry per unit length).

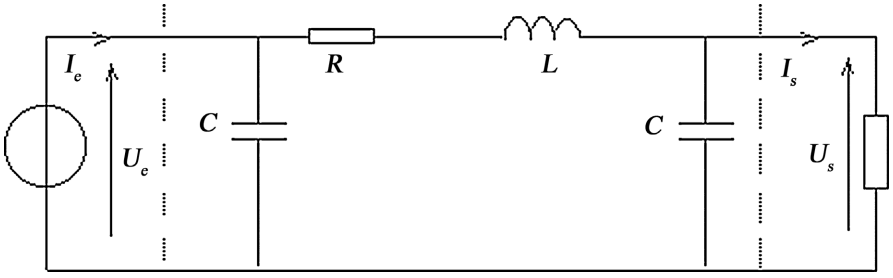

Figure 1. Simplified model of a high-voltage power line [28]-[30].

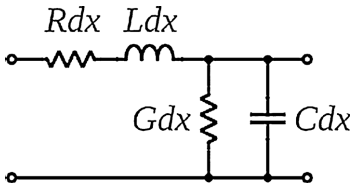

Figure 2. Two-port network model of a high-voltage power line [36]-[40].

- The linear capacitance C between the two conductors is represented by a shunt capacitor C (Farad per unit length).
- The linear conductance G of the dielectric medium separating the two conductors is represented by a shunt resistance (Siemens per unit length). The resistance in this model has a value of $1/G$ Ohms.

In this model, the voltage at any point a distance x from the beginning of the line is defined, and at any time t, the voltage $U(x,t)$ and the current $I(x,t)$ are defined. The equations can be written [36]-[40]:

$$\begin{cases} \dfrac{\partial U}{\partial x}(x,t) = -L\dfrac{\partial I}{\partial t}(x,t) - RI(x,t) \\ \dfrac{\partial I}{\partial x}(x,t) = -C\dfrac{\partial U}{\partial t}(x,t) - GU(x,t) \end{cases} \tag{21}$$

From the formulation above, we can derive two partial differential equations, each involving only one variable [36]-[40]:

$$\begin{cases} \dfrac{\partial^2 U}{\partial x^2}(x,t) = LC\dfrac{\partial^2 U}{\partial t^2}(x,t) + (RC+GL)\dfrac{\partial U}{\partial t}(x,t) + GRU(x,t) \\ \dfrac{\partial^2 I}{\partial x^2}(x,t) = LC\dfrac{\partial^2 I}{\partial t^2}(x,t) + (RC+GL)\dfrac{\partial I}{\partial t}(x,t) + GRI(x,t) \end{cases} \tag{22}$$

High-Voltage Line Parameters

The calculation of the electrical parameters used for modelling is based on Maxwell's equations. The model with a single Pi section is only valid for low frequencies and short power lines; otherwise, several Pi sections must be connected in series [34]-[37].

1) Resistance model

Starting from the local Ohm's law in local form [40]:

$$\boldsymbol{j} = \delta E \tag{23}$$

or:

$\boldsymbol{j}$: Current density (A/m^2);

δ : Electrical conductivity (Ω^{-1});

E : Electric field strength (V/m).

The resistance of conductors depends on temperature and frequency; it is defined by [39]-[40]:

$$R = \frac{l}{GS} = \frac{\rho l}{s} \tag{24}$$

The resistivity of a material increases with temperature according to the follow-

ing law.

$$\rho = \rho_o (1 + \alpha \Delta t) \tag{25}$$

or:

α : The coefficient of thermal expansion;

Δt : The temperature change in ˚C;

ρ_o : is the resistivity of the conductor at 20˚C (Ωm).

$$R = \frac{\rho_o (1 + \alpha \Delta t) l}{s} \tag{26}$$

2) Inductance Model

A conductor carrying a varying current "I" generates a magnetic flux "φ". The variation of this flux is the cause of the appearance of induced voltage. To account for these effects, the linear inductance of a conductor alone is defined as follows [36]-[40]:

$$L = \frac{\varphi}{I} = \frac{\mu_0}{2\pi}\left(\ln\frac{2h}{D} + \frac{1}{4n}\right) \tag{27}$$

With: h(m): height of the line relative to the ground. D(mm): diameter of the conductor. n: Number of conductors in the bundle [36]-[40].

3) Capacitance Model

The electric field established between the line and ground is the cause of the appearance of capacitive current (leakage current). To account for these effects, capacitance is defined as follows [36]-[40]:

$$C = \frac{Q}{v} = \frac{2\pi\varepsilon_0}{\ln\frac{D}{h}} \tag{28}$$

where: C is the line capacity in Farads; Q is the electrical charge carried by the line in Coulombs; and v is the line voltage in kV.

2.2. Simplified Models of AC HV Lines with Uniformly Distributed Constants

In electrical engineering, each electrical circuit can be represented as a four-terminal network, for which the constants A, B, C, and D, which link the input and output parameters, must be mathematically determined (see **Figure 3**) [36].

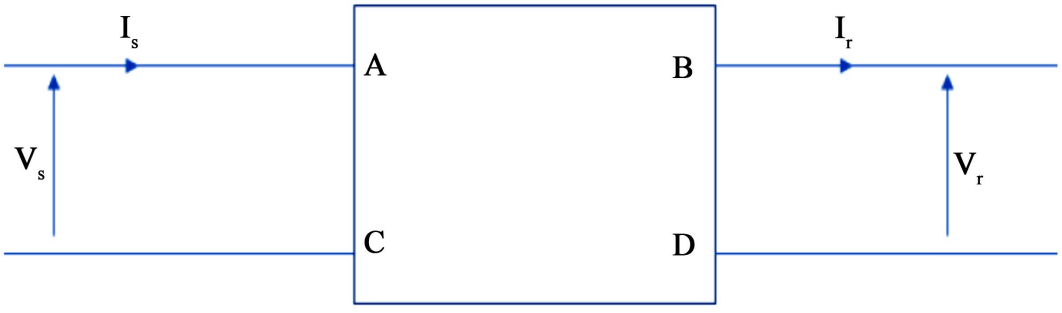

Figure 3. Power line represented by a two-port network [41]-[44].

From Figure 3 associated with the theory of two-port networks, the general equations are [45] [46]:

$$V_1 = AV_2 + BI_2 \tag{29}$$

$$I_1 = CV_2 + DI_2 \tag{30}$$

The constants A, B, C, and D depend on the electrical parameters of the line and are generally complex numbers. These equations in matrix form can be written as follows [45]:

$$\begin{bmatrix} V_1 \\ I_1 \end{bmatrix} = \begin{bmatrix} A & B \\ C & D \end{bmatrix} \begin{bmatrix} V_2 \\ I_2 \end{bmatrix} \tag{31}$$

The validity of Equations (29), (30) is based on the possibility of representing the transport line by a linear, passive and bilateral network, which imposes [46]:

$$AD - BC = 1 \tag{32}$$

On the other hand, we can write [45] [46]:

$$\begin{cases} V_1 = V_2 + ZI_2 \\ I_1 = I_2 \end{cases} \tag{33}$$

Starting from Equations (29)-(33), we derive the values of the constants A, B, C, and D from the line considered [45] [46].

$$\begin{cases} A = 1 \\ B = Z \\ C = 0 \\ D = 1 \end{cases} \tag{34}$$

Hence:

$$\begin{bmatrix} V_1 \\ I_1 \end{bmatrix} = \begin{bmatrix} 1 & Z \\ 0 & 1 \end{bmatrix} \begin{bmatrix} V_2 \\ I_2 \end{bmatrix} \tag{35}$$

The π model stipulates that the capacitance of the line is divided into two parts, $C/2$ each, which are connected to the two ends of the line, while the resistance and inductive reactance (series impedance of the line) of the line are totally concentrated in the center of the line as shown in the electrical diagram below Figure 4 [47]-[49].

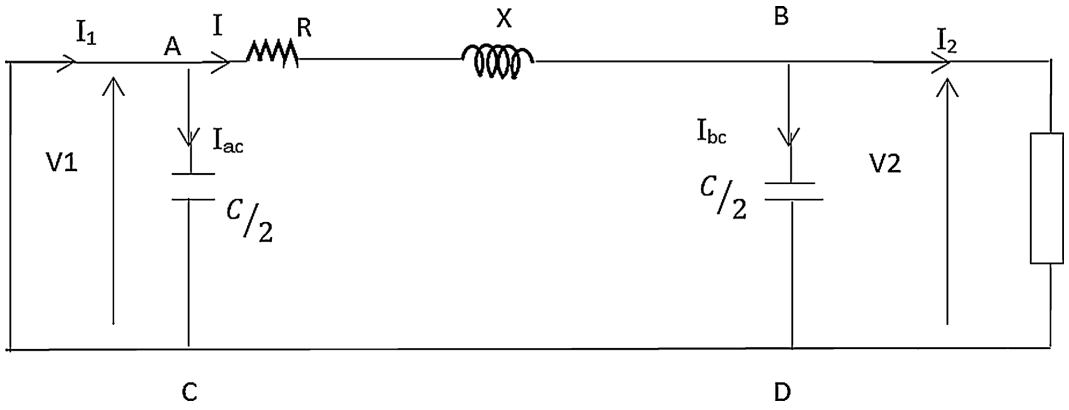

Figure 4. The π model of a long-distance AC high-voltage line [47]-[49].

From the electrical model in **Figure 4**, by applying Kirchhoff's current law at current node "A", the current I flowing through branch "AC" is therefore of the form [49]:

$$I = I_2 + I_{bd} = I_2 + \frac{Y}{2}V_2 \tag{35}$$

The source voltage is modeled by the following relationship [47]-[49]:

$$V_1 = V_2 + Z \cdot I \tag{36}$$

It can be shown from **Figure 4** that [48]:

$$V_1 = \left(1 + \frac{ZY}{2}\right)V_2 + Z \cdot I_2 \tag{37}$$

The current source is given by the following Equation (38):

$$I_1 = I + I_{cd} = I + \frac{Y}{2}V_1 \tag{38}$$

or:

$$\begin{cases} V_1 = \left(1 + \frac{ZY}{2}\right)V_2 + ZI_2 \\ I_1 = Y\left(1 + \frac{ZY}{4}\right)V_2 + \left(1 + \frac{ZY}{2}\right)I_2 \end{cases} \tag{38}$$

In matrix notation, Equation (39) can be written as follows [48] [49]:

$$\begin{bmatrix} V_1 \\ V_1 \end{bmatrix} = \begin{bmatrix} \left(1 + \frac{ZY}{2}\right) & Z \\ y\left(1 + \frac{ZY}{4}\right) & \left(1 + \frac{ZY}{2}\right) \end{bmatrix} \begin{bmatrix} V_2 \\ I_2 \end{bmatrix} = \begin{bmatrix} A & B \\ C & D \end{bmatrix} \begin{bmatrix} V_2 \\ I_2 \end{bmatrix} \tag{40}$$

Also, the constants A, B, C, and D of the network of an electrical line in the π model are deduced from the following expression (41) [49]:

$$\begin{cases} A = D = \left(1 + \frac{ZY}{2}\right) \\ B = Z \\ C = Y\left(1 + \frac{ZY}{2}\right) \end{cases} \tag{41}$$

Let the uniformly distributed constants of line [50] be denoted by R: resistance in (Ω); L: inductance in (H); G: conductance in (Ω^{-1}), and C: capacitance of one phase in (μF). We define Z (impedance) and Y (admittance) by the system of Equations (42) following [51].

$$\begin{cases} Z = R + jL\omega \\ Y = G + jC\omega \end{cases} \tag{42}$$

The operating equations of the lines with uniformly distributed constants characterising V_1 and I_1 at the input of the AC HV line, established from the solution of Equations (21) and (22), are then given by the expressions (43), (44) [51]:

$$V_1 = V_2 \cdot \cosh a + Z_0 \sinh a \cdot I_2 \tag{43}$$

$$I_1 = V_2 \cdot \frac{1}{Z_0} \cdot \sinh a + I_2 \cdot \cosh a \tag{44}$$

If we consider that:

$$a = \sqrt{Z \cdot Y} \cdot l \tag{45}$$

$$Z_0 = \sqrt{\frac{Z}{Y}} \tag{46}$$

And, as we know that, $\cosh^2 a - \sinh^2 a = 1$, Equations (43) and (44) satisfy the passive two-port network equation.

For the transmission of electrical energy over very long distances, the Joule effect must be minimised, and consequently, the ohmic resistance (R) and conductance (G) are extremely low and negligible compared to ($jL\omega$ and $jC\omega$). Furthermore, all high-voltage lines are constructed with a surface potential gradient of the conductors well below the critical gradient in order to reduce losses due to the corona effect. Lateral losses in the insulators are also negligible. In short, we can write [45].

$$\begin{cases} Z = jL\omega \\ Y = jC\omega \end{cases} \tag{47}$$

Taking into account these relationships, the quantity (a) defined by Equation (45), we therefore find:

$$a = j\omega\sqrt{L \cdot C} \cdot l \tag{48}$$

Furthermore, the approximate models of expressions (27-28) are respectively [39] [40]:

$$L \cong 2\ln\left(\frac{S}{a'}\right)10^{-5} \quad \text{in H/km} \tag{49}$$

If we neglect the internal flux of the cables.

$$C \cong \frac{10^{-6}}{18\ln\left(\frac{S}{a'}\right)} \quad \text{in F/km} \tag{50}$$

In these expressions, (a') is the fictitious equivalent radius of a beam of (n) conductors and (a') is given by:

$$a' = r \cdot \sqrt{n\left(\frac{D}{2r}\right)^{n-1}} \tag{51}$$

or:

r: is the outer radius of the cable used in mm, S: is the equivalent phase spacing in mm, and D: is the conductor diameter in mm.

This phase spacing can be determined by [39] [40] [45]:

$$S = \sqrt[a]{S_{12} \cdot S_{18} \cdot S_{28}} \tag{52}$$

Multiplying terms (49-50) gives the value of 3.10^5, which is close to the numer-

ical value of the speed of light and, given the units used, is indeed (c) the speed of light.

$$L \cdot C = \frac{1}{\left(3 \times 10^5\right)^2} \tag{53}$$

Under these conditions (48) is transformed as follows:

$$a = j \cdot 2\pi \cdot f\left(\frac{1}{c}\right) \cdot l = j2\pi \frac{l}{c:f} = j2\pi \frac{l}{\lambda} \tag{54}$$

where (λ) is the wavelength of the sinusoidal alternating current, which, if f = 50 hertz, is 300,000 ÷ 50 = 6000 km. Therefore, we finally have:

$$a = j \cdot 2\pi \frac{l}{6000} \tag{55}$$

According to [45], complex hyperbolic equations possess the mathematical property of equivalence with ordinary trigonometric functions given by:

$$\cosh jx = \cos x \tag{56}$$

$$\sinh jx = j \sin x \tag{57}$$

2.3. Modelling of No-Load Overvoltage Induced by Electromagnetic Fields (EMFs)—Capacitive and Inductive Effects

Taking into account expressions (43-44) and Equations (55)-(57), the simplified form of equations (43-44) is:

$$V_1 = V_2 \cdot \cos\left(2\pi \frac{l}{6000}\right) + I_2 \cdot jZ_0 \sin\left(2\pi \frac{l}{6000}\right) \tag{58}$$

$$I_1 = V_2 \cdot j \cdot \frac{1}{Z_0} \sin\left(2\pi \frac{l}{6000}\right) + I_2 \cdot \cos\left(2\pi \frac{l}{6000}\right) \tag{59}$$

For a high-voltage AC line operating at no load, I_2 = 0 and Equation (58) becomes:

$$V_1 = V_2 \cdot \cos 2\pi \frac{l}{6000} \tag{60}$$

Equation (60) shows that, for (l) equal to 1000 km, the voltage at the end of the AC HV line is twice that of the input:

$$V_2 = 2V_1 \tag{61}$$

When alternating current power transmission lines exceed a certain length, as shown in Equation (60), they become sensitive to distance and frequency, generating electromagnetic waves. These waves are the basis of capacitive and inductive effects that can cause high no-load overvoltages of almost 200%.

For (l) reaching a quarter-wavelength, *i.e.*, 1500 km, the overvoltage is infinite. For (l) exceeding a quarter-wavelength, the overvoltages along the line take on excessive values when the line is unloaded [45]-[57].

2.4. Compensation Model for High Voltage AC Lines Subject to High No-Load Overvoltage

Assume that the series capacitor C_1 is inserted at the end of the line and that the resulting situation is that defined by the following **Figure 5** [45]:

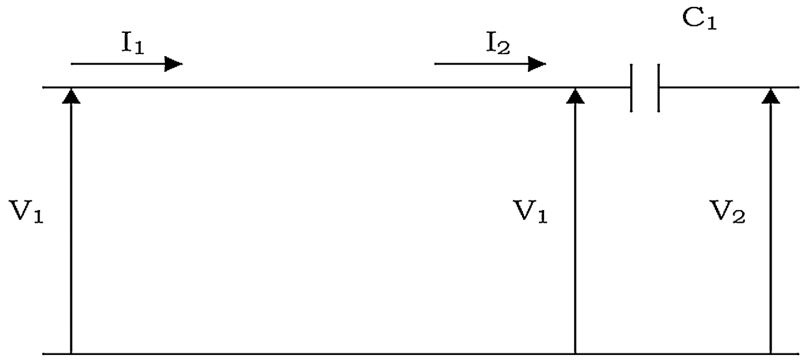

Figure 5. Insertion of a serial capacitor C_1 at the end of a line segment considered in (n) segments. [45]-[58].

The vector equations relating to **Figure 5** are:

$$V_1 = AV' + BI_2 \tag{62}$$

$$I_1 = CV' + DI_2 \tag{63}$$

$$V' = V_2 - j\frac{I_2}{C_1\omega} \tag{64}$$

By eliminating V' we have:

$$V_1 = A \cdot V_2 + B_1 \cdot I_2 \tag{65}$$

$$I_1 = C \cdot V_2 + D_1 \cdot I_2 \tag{66}$$

or:

$$B_1 = B - j\frac{A}{C_1\omega} \tag{67}$$

$$D_1 = D - j\frac{C}{C_1\omega} \tag{68}$$

Equations (65) and (66) obviously satisfy expressions (29)-(30). Let us adopt the following simplified expressions as equations of the lines:

$$A = D = \cos\left(2\pi\frac{l}{6000}\right) \tag{69}$$

$$B = j \cdot Z_0 \cdot \sin\left(2\pi\frac{l}{6000}\right) \tag{70}$$

$$C = j\frac{1}{Z_0} \cdot \sin\left(2\pi\frac{l}{6000}\right) \tag{71}$$

For very long lines, the capacitive current is significant. It causes overvoltages (see Equation (60)), which can be excessive, and it is necessary to cancel this ca-

pacitive current completely or partially. An insertion (or several suitably distributed along the line) of a shunt reactance can serve this purpose. Suppose we introduce a shunt reactance X at the incoming end of the line in Figure 5, where the capacitor C_1 is inserted. The resulting situation will be that of Figure 6 below, allowing us to deduce the vector equation below:

$$I_1 = AV_2 + D_1\left(\frac{V_2}{jX} + I_2'\right) = \left(C + \frac{D_1}{jX}\right)V_2 + D_1 I_2' \tag{72}$$

The presence of the shunt reactance in Figure 6 allows the HTAC line to be artificially transformed into a DC connection, with A being negligible. This results in compensation of the capacitive current I_2, provided the line is not compensated at 100%. Consequently, at no load, $I_2' = 0$, and the overvoltage at the end of the line is therefore reduced (see Equation (73)).

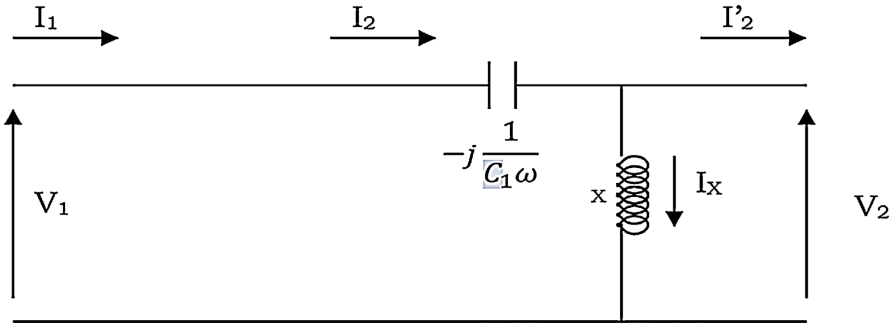

Figure 6. Insertion of a shunt reactance X at the end of a line (or line segments).

$$I_1 = \left(C + \frac{D_1}{jX}\right)V_2 \tag{73}$$

Therefore, the capacitive current of the line, equal to $C \cdot V_2$, is reduced and could even become inductively reactive, which is not desirable. For a long line, the introduction of a shunt reactance produces an overly abrupt concentrated effect, and it is more appropriate to distribute the insertions of shunt reactances and series capacitors evenly along the line. Consider a line of length (L) divided into (n) equal segments. Let (d) be the length of a segment. We have [29]:

$$l = n \cdot d \tag{74}$$

In a practical implementation, the intersection points could be determined in a mandatory manner:

- Presence of an electrical power supply station. The intersection of the reactances and capacitors should preferably be made at such a location because it is under surveillance, and the connection would also be less expensive.
- Geographical (topographical) impossibility of easily accessing the theoretical intersection point. For example, a river crossing at that location or the presence of a mountain that is difficult to access.
- Favourable location for accessing such a point due to the presence of a road, railway, or navigable river.

If this is the case, Equation (74) will be replaced by the following expression (75):

$$l = d_1 + d_2 = d_3 + \cdots + d_n \tag{75}$$

To illustrate our ideas, we will consider the simple case of dividing the line into (n) equal segments. For segment (1)-(2) we have:

$$V_1 = A_1 V_2 + B_1 I_2 \tag{76}$$

And,

$$I_1 = C_1 V_2 + D_1 I_2 \tag{77}$$

And the insertion node of the shunt reactance *X*, we have:

$$I_2 = I_2' + \frac{V_2}{jX} \tag{78}$$

Following the same reasoning, for the segment (2)-(3), we have:

$$V_2 = A_2 V_3 + B_2 I_3 \tag{79}$$

and,

$$I_2 = C_2 V_3 + D_2 I_3 \tag{80}$$

Substituting V_2 and I_2' into Equations (76) and (77) with their expressions, we obtain the following results after grouping:

$$V_1 = \left(A^2 + \frac{AB_1}{jX} + BC \right) \cdot V_3 + \left(AB + \frac{B_1^2}{jX} + B_1 D_1 \right) I_3 = A' \cdot V_3 + B' I_3 \tag{81}$$

and similarly, I_1 is equal to:

$$I_1 = C' V_3 + D' I_3 \tag{82}$$

The next node at the end of the second segment is another reactance *X*, and we proceed in the same way as before. Finally, the various *A*, *B*, *C*, and *D* coefficients can be obtained from the algorithms shown in Table 1 below, clearly illustrating the general law governing the formation of the *A*, *B*, *C*, and *D* coefficients of the two-port network.

Table 1. Coefficients of the various equations as a function of the number of segments.

Segments	*A*	*B*	*C*	*D*
1 - 2 2 - 3 3 - 4 4 - 5	A	B_1	C	D_1
1 - 4 (')	$A^2 + \frac{AB_1}{jX} + B_1 C$	$AB_1 + \frac{B_1^2}{jX} + B_1 D_1$	$AC + \frac{AD_1}{jX} + CD_1$	$B_1 C + \frac{B_1 D_1}{jX} + D_1^2$
1 - 4 (")	$AA' + \frac{B'}{jY} + B'C$	$A'B_1 + \frac{B_1 B'}{jY} + B'D_1$	$AC' + \frac{AD'}{jY} + CD'$	$B_1 C' + \frac{B_1 D'}{jY} + D_1 D'$
1 - 5 ("')	$AA'' + \frac{AB''}{jZ} + B''C$	$A''B_1 + \frac{B_1 B''}{jZ} + B''D_1$	$AC'' + \frac{AD''}{jZ} + CD''$	$B_1 C'' + \frac{B_1 D''}{jZ} + D_1 D''$

2.5. Numerical Model of the EHV or HV AC Power Line

Obtaining the recurrence model for a high-voltage AC line segmented into n segments using the finite difference method relies on discretising the telegrapher's equations and applying an iterative four-pole formalism. The continuous transmission line is governed by the telegrapher's equations in the steady state (frequency f, angular frequency ω), as a function of the position x along the line:

$$\frac{\mathrm{d}V(x)}{\mathrm{d}x} = -Z \cdot I(x) \tag{83}$$

$$\frac{\mathrm{d}I(x)}{\mathrm{d}x} = -Y \cdot V(x) \tag{84}$$

where $Z = R + j\omega L$ is the series impedance per unit length, and $Y = G + j\omega C$ is the parallel admittance per unit length.

For a segment of length $\Delta x = L/n$, we approximate the derivatives at the discretisation points k and k+1 (where k varies from 0 to $n-1$):

Voltage: $\frac{V_{k+1} - V_k}{\Delta x} \approx -Z \cdot I_k$ (or a more precise centered approximation)

Current: $\frac{I_{k+1} - I_k}{\Delta x} \approx -Y \cdot V_{k+1}$ (or another approximation)

Modeling a segment (Elementary Quadripole)

The use of the chain of transfer matrices (ABCD or transmission matrices), where the total matrix $T_{tatol} = T_1 \cdot T_2 \cdots T_n$, links the input parameters (V_1, I_1) to the output parameters (V_{n+1}, I_{n+1}) via a recursive relation between each segment where, each segment i (length Δx) is represented by a transmission matrix T_i, the input parameters (V_i, I_i) and output parameters (V_{i+1}, I_{i+1}) are linked by the following relation (85):

$$\begin{pmatrix} V_i \\ I_i \end{pmatrix} = T_i \cdot \begin{pmatrix} V_{i+1} \\ I_{i+1} \end{pmatrix} \tag{85}$$

Recurrence relation for n segments

The complete line is a cascade of n transmission matrices T_i. If the segments are identical ($T_i = T$ for all i), the total matrix is:

$$T_{tatol} = T_1 \cdot T_2 \cdots T_n = T^n \tag{86}$$

The overall input/output relationship becomes:

$$\begin{pmatrix} V_1 \\ I_1 \end{pmatrix} = T_{tatol} \cdot \begin{pmatrix} V_{n+1} \\ I_{n+1} \end{pmatrix} = T_1 \cdot T_2 \cdots T_n \begin{pmatrix} V_{n+1} \\ I_{n+1} \end{pmatrix} = T^n \begin{pmatrix} V_{n+1} \\ I_{n+1} \end{pmatrix} \tag{87}$$

The recurrence model allows us to calculate the state of the row at any point by iteratively applying the matrix T based on the initial or final conditions. We note that the matrix T^n equals:

$$T^n = \begin{pmatrix} A_{n-1} & B_{n-1} \\ C_{n-1} & D_{n-1} \end{pmatrix} \tag{88}$$

Substituting expression (88) into Equation (87), we find:

$$\begin{pmatrix} V_1 \\ I_1 \end{pmatrix} = \begin{pmatrix} A_{n-1} & B_{n-1} \\ C_{n-1} & D_{n-1} \end{pmatrix} \begin{pmatrix} V_{n+1} \\ I_{n+1} \end{pmatrix} \tag{89}$$

From model (89), we can deduce the recurrence model for an HT AC line segmented into n segments.

$$V_1 = A_{n-1} \cdot V_{n+1} + B_{n-1} \cdot I_{n+1} \tag{90}$$

$$I_1 = C_{n-1} \cdot V_{n+1} + D_{n-1} \cdot I_{n+1} \tag{91}$$

The coefficients A_{n-1} and C_{n-1} define the no-load overvoltage at the end of the line, while B_{n-1} and D_{n-1} define the capacitive current.

3. Simulation Results

The main limitation in the analytical solution of the two-port network model applied to long-distance extra-high-voltage (EHV) lines lies in the complexity of the mathematical expressions involved. Indeed, the distributed representation of the line leads to equations involving hyperbolic functions (sinh, cosh), which become difficult to manipulate when the length exceeds a certain threshold, generally greater than 250 km. In this case, the electrical quantities exhibit a strong dependence on distance and frequency, further complicating any attempt at an analytical solution, particularly for asymmetrical configurations or when the line parameters are not constant.

This difficulty is also encountered in the calculation of compensation parameters, which vary directly with the number of segments considered in the model. Thus, in transient conditions, the use of a numerical solution becomes necessary, given that the analytical solution often becomes impractical or even nonexistent.

To achieve this, a numerical approach was chosen in this study, offering a more robust and suitable method for simulating the dynamic behaviour of long-distance EHV lines.

Our major contribution in this study is to present a numerical method for the dynamics of an EHV line, regardless of its length, to provide insight into its behaviour under overvoltage at the line's end, capacitive current in response to series capacitance compensation, and shunt reactance. The numerical method used in this study is based on Equations (72), (83), and (84) and the algorithms in Table 1. These equations are then solved using a MATLAB program. However, this approach will be validated by comparing the analytical results obtained from models (76)-(82).

3.1. Declaration of Characteristic Parameters of the AC EHV Line

- Line voltage: length U = 400 kV;
- Line length l = 1200 km;
- Line inductance L = 0.292 H/km;
- Line capacitance C = 3.58 × 10^{-6} F/km;
- Characteristic line impedance Z_0 = 286 Ω.

3.2. Results of the Analytical Approach

1) Parameters (*A*, *B*, *C* and *D*) of the Two-Port Network

The parameters of (*A*, *B*, *C* and *D*) of the four-terminal network modelling the AC high-voltage line in our study for the 3 scenarios are presented in Tables 2-4 below:

Table 2. Coefficients of the various equations as a function of the number of segments (Scenario 1: Case of $n = 4$ segments).

Segments	*A*	*B*	*C*	*D*
1 - 2	0.951	j 5.06 j 88.37	J 1.08×10^{-3}	0.856
1 - 3	0.9041	j 9.1709	j 0.0011	0.7319
1 - 4	0.8595	j 12.4749	j 0.0011	0.6251
1 - 5	0.816	j 15.0954	j 0.0011	0.533

Table 3. Coefficients of the various equations as a function of the number of segments (Scenario 2: Case of $n = 6$ segments).

Segments	*A*	*B*	*C*	*D*
1 - 2	0.978	j 85.9	j 0.73×10^{-3}	0.935
1 - 3	0.9572	j 4.4919	j 4.1429×10^{-4}	0.8749
1 - 4	0.9369	j 6.456	j 1.2479×10^{-4}	0.8192
1 - 5	0.9184	j 8.2497	–j 1.405×10^{-4}	0.7678
1 - 6	0.9008	j 9.8878	–j 3.8346×10^{-4}	0.7201
1 - 7	0. 8842	j 11.3825	–j 6.058×10^{-4}	0.6760

Table 4. Coefficients of the various equations as a function of the number of segments (Scenario 3: Case of $n = 8$ segments).

Coefficients/Segments	*A*	*B*	*C*	*D*
1 - 2	0.987	j 1.38 (B1)	j 0.54×10^{-3}	1.0106
1 - 3	0.9749	j 2.7587	j 7.316×10^{-6}	1.0221
1 - 4	0.9629	j 4.1374	–j 5.244×10^{-4}	1.0344
1 - 5	0.9526	j 5.5162	–j 0.0011×10^{-4}	1.0476
1 - 6	0.9431	j 6.8974	–j 0.0016×10^{-4}	1.0617
1 - 7	0.9344	j 8.282	–j 0.0021×10^{-4}	1.0768
1 - 8	0.9265	j 9.671	–j 0.0027×10^{-4}	1.0927
1 - 9	0.9195	j 11.067	–j 0.0032×10^{-4}	1.1096

2) Voltage and Capacitive Current Behaviour at the End of the EHV Line

By implementing models (76)-(82) in the Matlab environment, we obtain the analytical results presented in the following Figures 7-9:

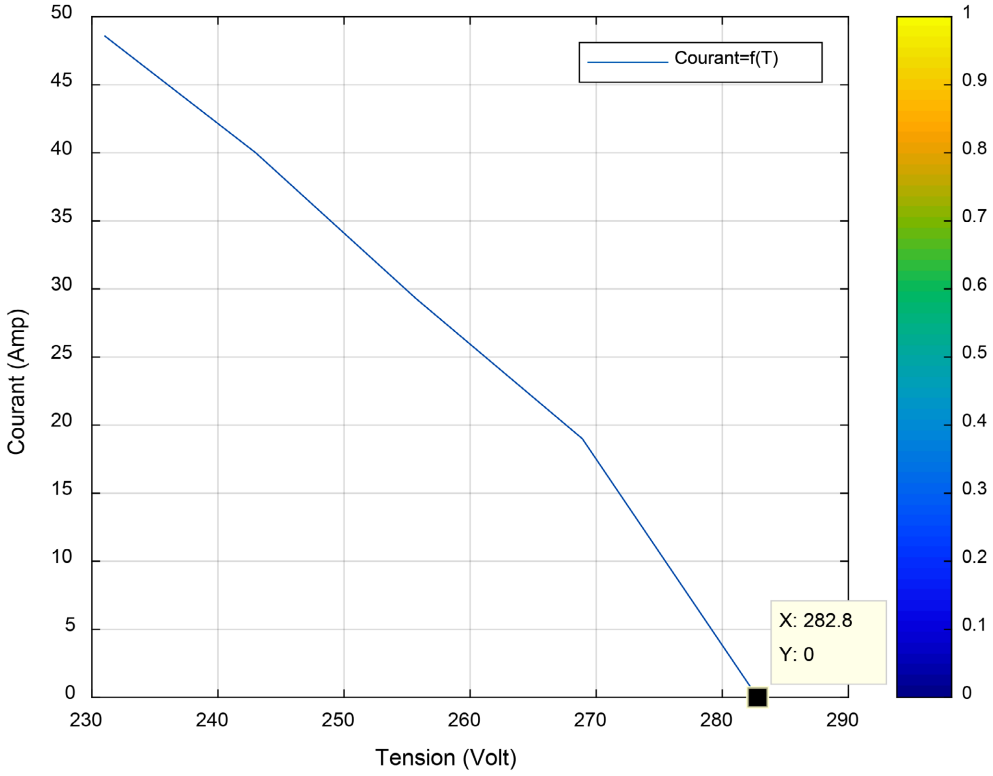

Figure 7. Variation of current as a function of voltage (Scenario 1: Case of $n = 4$ segments).

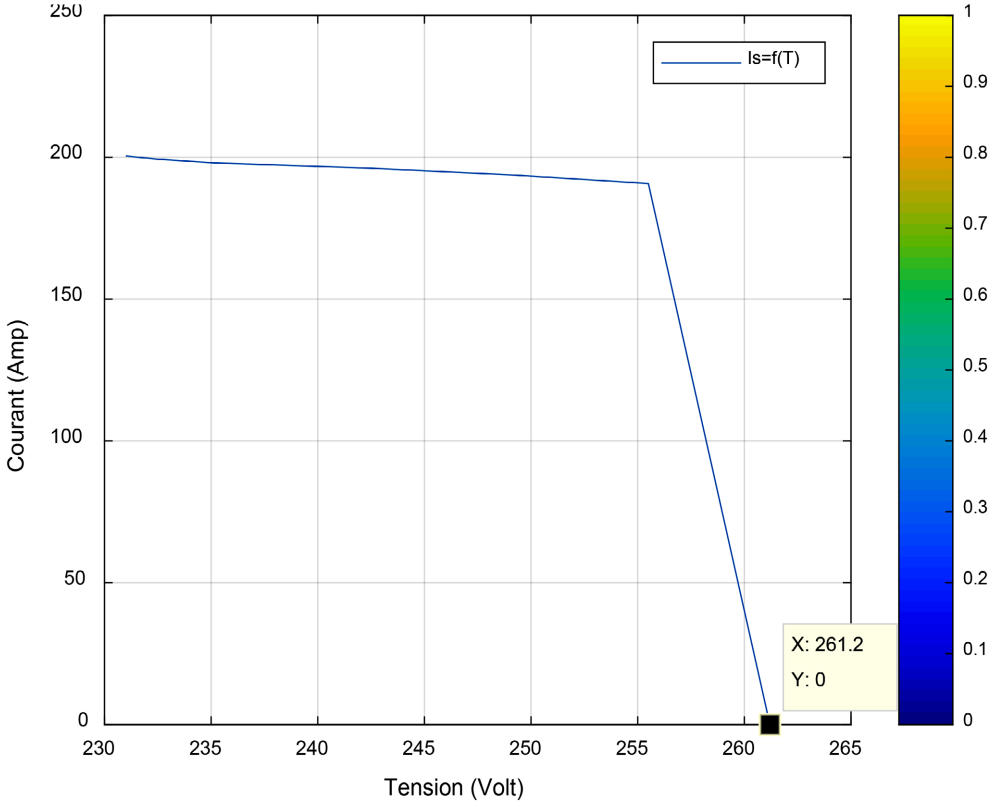

Figure 8. Voltage variation as a function of current for a line arranged in six sections (Scenario 2: Case of $n = 6$ sections).

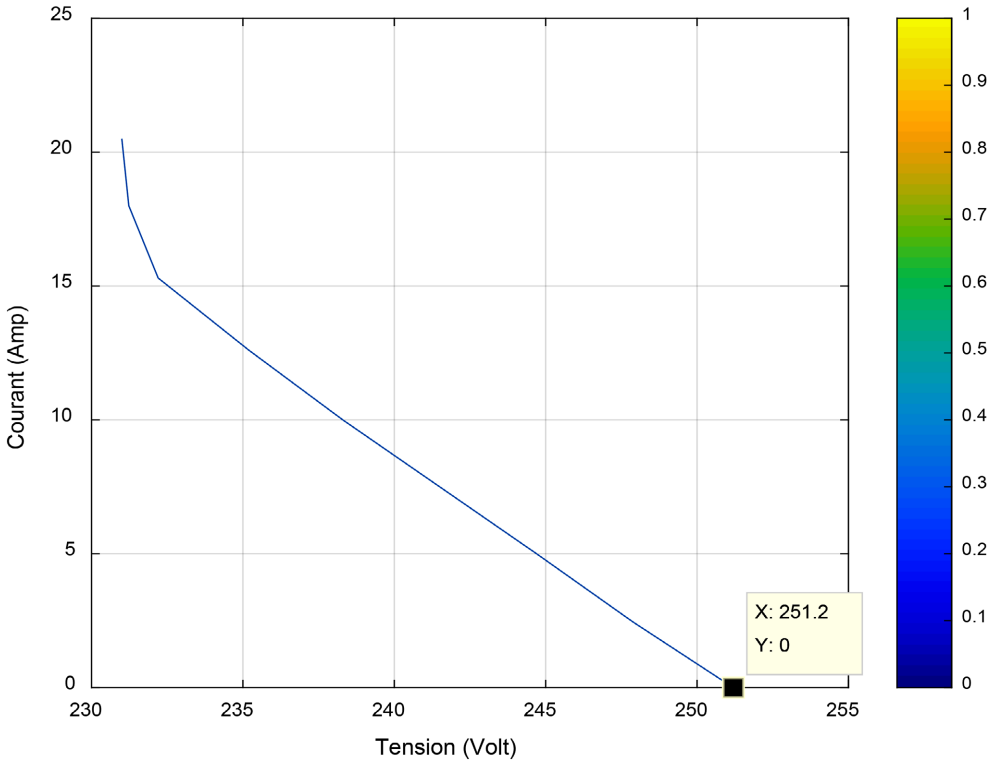

Figure 9. Voltage variation as a function of current for a line divided into eight sections (Scenario 1: Case of $n = 8$ sections).

3.3. Results of Numerical Approach

1) Parameters (A, B, C, and D) of the Two-Port Network

The parameters (A, B, C, and D) of the two-port network modeling the AC high-voltage transmission line in our study for the 3 scenarios are presented in Figures 10-12 below.

2) Voltage and Capacitive Current Behaviour at the Output of the EHV Line

By clicking the "display voltage-current curves" interface shown in the GUI interface of Figures 10-12, we obtain the analytical results presented in the following Figures 13-15 and Table 5.

4. Discussions

The effects of electromagnetic waves on long-distance high-voltage AC power lines are a current topic of interest, as the presence of magnetic and electric fields around transmission lines can lead to capacitive and inductive effects. These phenomena are inherent to the operation of power lines and can intensify over long distances due to the accumulation of electrical charges and electromagnetic induction, thus affecting the network and causing disturbances. The combination of capacitive and inductive effects can lead to transient overvoltages or switching overvoltages, which can impact the stability of the electrical system.

To obtain the results of various simulations, the four-port network model derived from Maxwell's and telegraphers' equations was used for the analytical

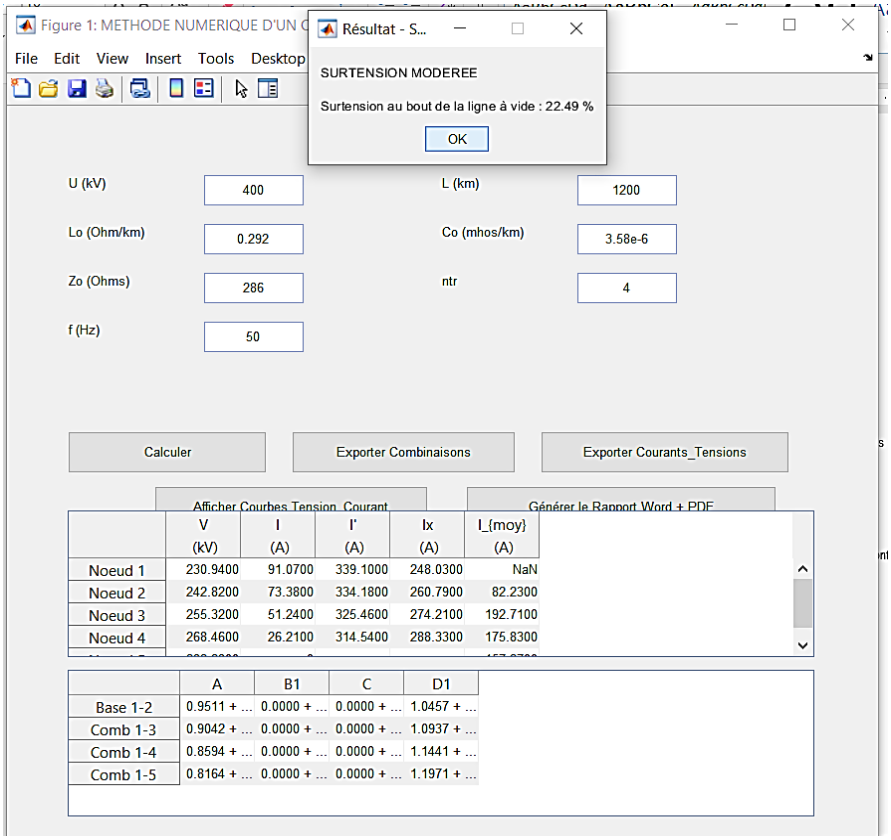

Figure 10. Scenario 1: Case of $n = 4$ segments.

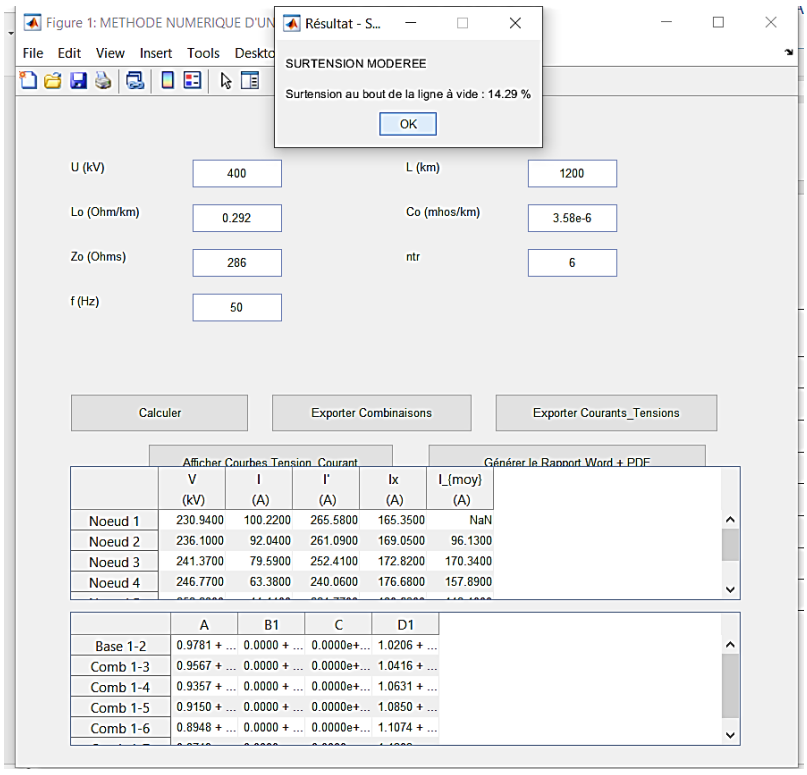

Figure 11. Scenario 2: Case of $n = 6$ segments.

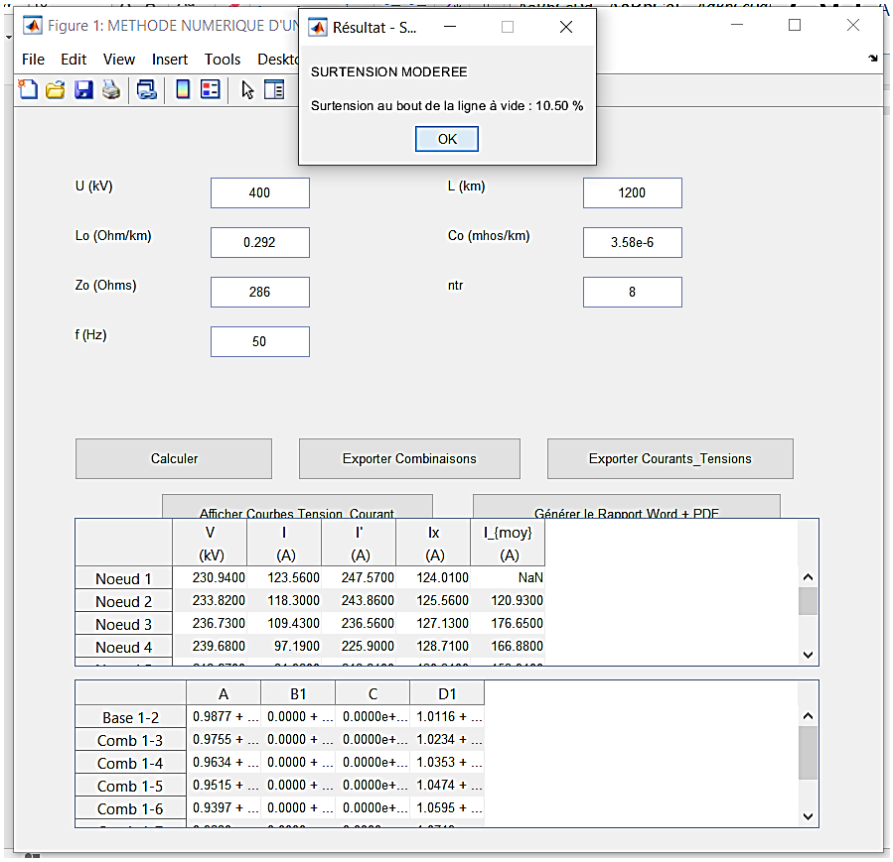

Figure 12. Scenario 3: Case of $n = 8$ segments.

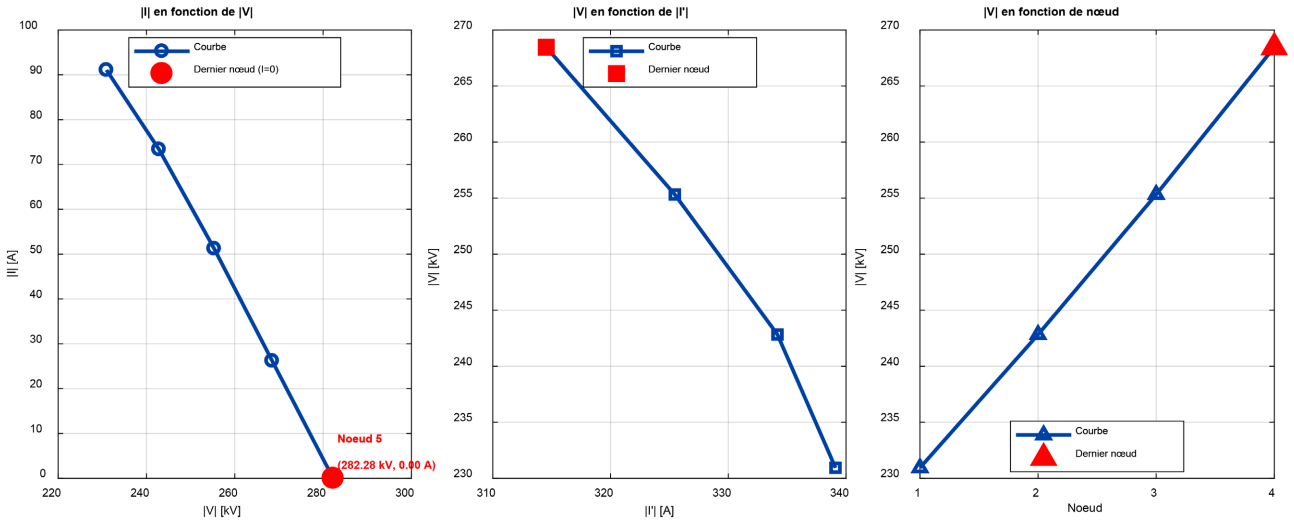

Figure 13. Voltage and capacitive current behavior at the output of the EHT line (Scenario 1: Case of $n = 4$ sections).

and numerical modeling of the problem addressed in this article. To this end, the following results were obtained:

Tables 2-4 show that the coefficients A, B, C, and D of the two-port network modeling the line as a function of its characteristic parameters decrease with increasing numbers of samples n (number of segments).

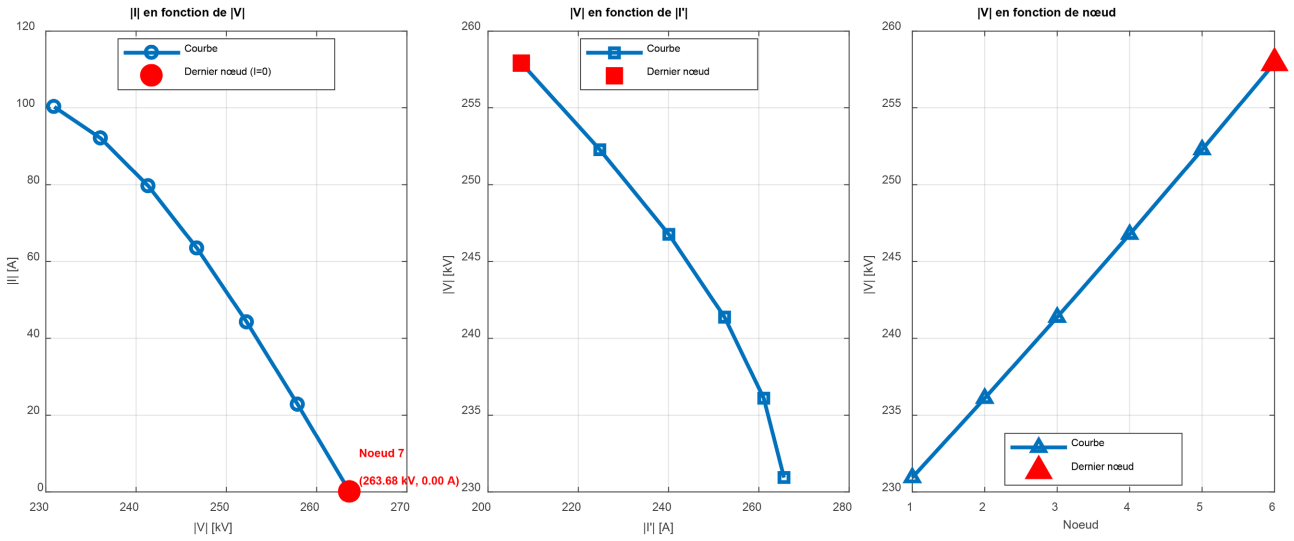

Figure 14. Voltage and capacitive current behavior at the output of the EHT line (Scenario 2: Case of $n = 6$ sections).

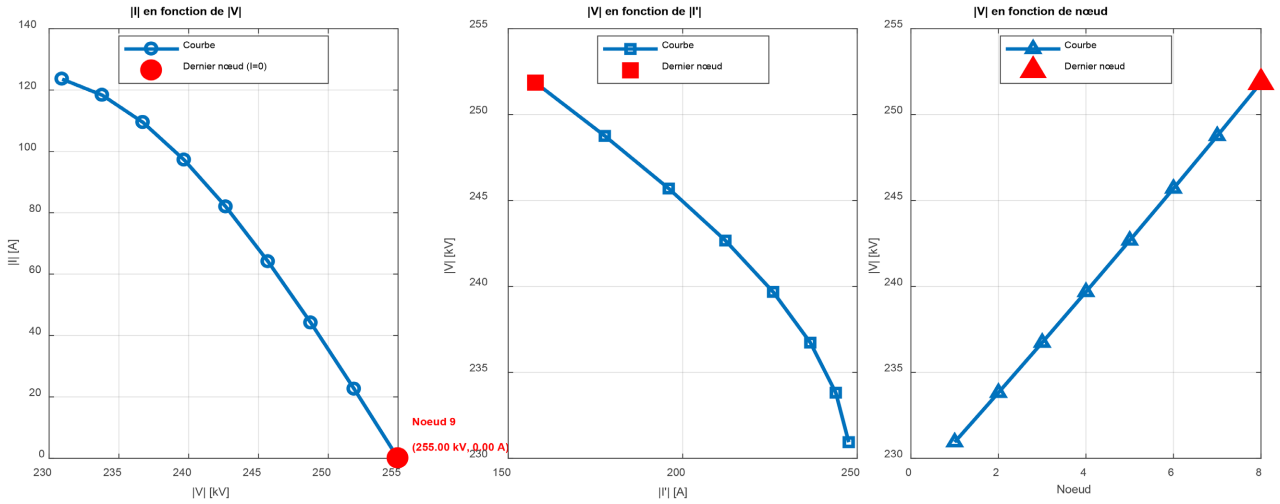

Figure 15. Voltage and capacitive current behavior at the output of the EHT line (Scenario 3: Case of $n = 8$ sections).

Table 5. Comparison of overvoltage results at the output of the HV line.

Number of segments	Analytical Method	Numerical Method	Difference
4 segments	22%	22.29%	0.29%
6 segments	13%	14.29%	1.29%
8 segments	8%	10.5%	2.5%
10 segments	-	8.31%	-
12 segments	-	6.87%	-
14 segments	-	5.87%	-

Figure 7 shows the variation of the capacitive current as a function of the voltage at the end of the line for the case of $n = 4$ segments. We observe a phase-to-ground voltage at the end of the line of 282.8 kV, representing an overvoltage of

22% once the line is divided into 4 segments by the insertion of a compensator. This overvoltage is unacceptable according to current standards.

Figure 8 visualises the capacitive current profile as a function of the voltage at the end of the line for the case of $n = 6$ segments. We observe a phase-to-phase voltage of 261.2 kV at the end of the line, representing a 13% overvoltage once the line is divided into 6 segments by the insertion of compensators. This overvoltage is also unacceptable according to current standards.

However, Figure 9 simulates the variation of the capacitive current as a function of the voltage at the end of the line for the case of $n = 8$ segments. As can be seen, the phase-to-phase voltage at the end of the line is 251.2 kV, representing an 8% overvoltage once the line is divided into 8 segments by the insertion of compensators. This overvoltage is also unacceptable according to current standards. Therefore, the overvoltage at the end of the line is inversely proportional to the number of compensator insertion points.

Figures 10-12 present the user interfaces generated by the root program developed in MATLAB. These tables allow for the numerical calculation of the ABCD coefficients of the two-port network modeling the line as a function of its characteristic parameters. The results corroborate those presented in Tables 2-4. We also observe that these coefficients decrease with increasing numbers of samples n (number of segments).

Figures 13-15, obtained using the numerical approach, present the results of the capacitive voltage-current behaviour at the end of the high-voltage AC line configured with 4, 6, and 8 segments. Figure 13 shows a phase-to-phase voltage at the end of the high-voltage AC line of 282.28 kV, representing an overvoltage of 22.49%; Figure 14 shows a phase-to-phase voltage at the end of the high-voltage AC line of 263.68 kV, representing an overvoltage of 14.29%; and finally, Figure 15 shows a phase-to-phase voltage at the end of the high-voltage AC line of 255 kV, representing an overvoltage of 10.5%. These results are close to those of Figures 7-9 obtained by the analytical approach, as shown in Table 5, which presents the percentage errors of overvoltages recorded by comparing the two methods. For a 1200 km AC high-voltage line segmented into 04 sections, we observe an overvoltage error of 0.029, or 0.29%; for 06 sections, an overvoltage error of 0.0129, or 1.29%; and finally, for 08 sections, an overvoltage error of 0.025, or 2.5%. The root mean square error for these three scenarios is 2.6%, a value less than 5% as required by the standard (RMSE) [57]. We can thus confirm the validity of our results obtained by the numerical approach.

Although the proposed models give realistic results, their potential limitations lie in the assumption of linear components; non-linear phenomena such as the corona effect, rapid transients such as lightning, and complex couplings (proximity effects) are not accounted for in the modeling.

5. Conclusions

The global energy market is characterised by two major trends: sustained demand

growth and the increasing distance between production centres and consumption areas. In this context, alternating current (AC) power transmission lines, when they cover long distances, exhibit electrical phenomena that are highly dependent on distance and frequency. This dependence promotes the propagation of electromagnetic waves, generating capacitive and inductive effects that can cause no-load overvoltages and various disturbances in the grid. Reducing these undesirable effects related to electromagnetic wave propagation in long-distance power transmission raises essential issues concerning the quality of electrical power.

Controlling overvoltage phenomena, in particular, is a major challenge for ensuring voltage and power stability during transmission.

To address these constraints, the use of series or parallel compensation devices provides an effective solution for mitigating the disruptive phenomena associated with long transmission lines. The objective of this article is to study, through simulation, the impact of electromagnetic waves on a long-distance AC transmission line, with a view to reducing no-load overvoltage stresses. To this end, we compared two approaches: analytical and numerical, to model and predict observed overvoltages and evaluate their attenuation conditions.

This article focused on the case of a 1200 km line where we conducted a study of line configurations with 4, 6, and 8 segments, incorporating series capacitors and shunt reactances to improve network stability. After applying two methods, we obtained the following results:

- A configuration with four (4) segments resulted in an overvoltage of 282.28 kV at the end of the line, representing an overvoltage of 22.49%. Unlike the analytical method, which resulted in an overvoltage of 282.8 kV, or 22%.
- A six-section configuration reduced the overvoltage to 263.68 kV, or 14.29%; in contrast, the analytical method resulted in an overvoltage of 261.2 kV, or 13%.
- To significantly improve stability, a shunt configuration (8 sections) was considered, resulting in an overvoltage at the end of the line slightly lower than the 10% recommended by the IEC standard. However, the numerical method achieved an acceptable overvoltage for a ten-section configuration.

The results of the various 2D simulations obtained demonstrate that the analytical approaches and computer tools used are satisfactory.

In future research, we plan a comparative study using the Russian method, which applies insertion and that of the Americans by inserting the Shunt reactances at both ends of the line.

Conflicts of Interest

The authors declare no conflicts of interest regarding the publication of this paper.

References

[1] Hossain, F. and Chaudhuri, N.R. (2025) A Dynamic Phasor Framework for Analysis of Grid-Forming Converter Connected to Series-Compensated Line. 2025 *IEEE*

Power & Energy Society General Meeting (*PESGM*), Austin, 27-31 July 2025, 1-5. https://doi.org/10.1109/pesgm52009.2025.11225603

[2] Saied, M.M. (2024) Electromagnetic Transients in Compensated Power Lines—Revisited: New Approach and Case Studies. *International Journal of Electrical and Communication Engineering Technology*, **2**, 19-26.

[3] Saied, M.M. (2023) The Electromagnetic Transients in Compensated High Voltage Power Lines. *International Journal of Electrical Power and Machine Systems*, **1**, 1-8.

[4] Ordóñez, C.A., Gómez-Expósito, A. and Maza-Ortega, J.M. (2021) Series Compensation of Transmission Systems: A Literature Survey. *Energies*, **14**, Article 1717. https://doi.org/10.3390/en14061717

[5] Balci, M. and Aydin, M. (2017) Electromagnetic Analysis of Power Systems: Fundamentals and Applications. Springer.

[6] Paul, C.R., Nasar, S.A. and Unnikrishnan, K.P. (2016) Introduction to Electromagnetic Compatibility. 4th Edition, John Wiley & Sons.

[7] Jelinek, L. and Kotek, T. (2015) Numerical Methods for Electromagnetic Fields in Electrical Engineering. CRC Press.

[8] Popov, M. (2017) Power System Transients: Parameter Determination. Springer.

[9] Belmans, R., *et al.* (2016) Numerical Simulation of Electromagnetic Transients in HVAC High-Voltage Transmission Lines Using FDTD Method. *IEEE Transactions on Power Delivery*, **31**, 1789-1797.

[10] Chen, Y., *et al.* (2015) FEM-Based Electromagnetic Field Analysis of HVAC Transmission Lines: Impact on Nearby Communication Cables. *Electric Power Systems Research*, **127**, 145-153.

[11] Gao, C., *et al.* (2018) Maxwell's Equations-Based Modeling of Electromagnetic Interference in UHV AC Transmission Lines. *International Journal of Electrical Power & Energy Systems*, **99**, 342-350.

[12] Martínez, J., *et al.* (2017) Numerical Analysis of Electromagnetic Fields around HVAC Transmission Lines: A Comparison between FDTD and MoL Methods. *Journal of Electromagnetic Waves and Applications*, **31**, 781-798.

[13] Wang, H., *et al.* (2015) Electromagnetic Transient Simulation of UHV AC Transmission Lines Considering Soil Ionization. *IEEE Transactions on Electromagnetic Compatibility*, **57**, 1356-1364.

[14] CIGRE Working Group 33.01 (2016) Electromagnetic Environment of High-Voltage AC Transmission Lines. CIGRE Technical Brochure 654.

[15] IEC 61000-4-20 (2018) Electromagnetic Compatibility (EMC)—Part 4-20: Testing and Measurement Techniques—Emission and Immunity Testing in Transverse Electromagnetic (TEM) Waveguides.

[16] AEG (1970) Telefunken, BBC, Siemens. Bulletin n˚5.

[17] Leroux, D. (2005) Electrical Characteristics of the Elements of a Transmission Network. Polytechnique School of Montreal, Canda.

[18] TCCHT Working Group (1970) Further Studies on Experimental Valves for the Transport of High-Voltage Direct Current in the Mamhein-Rhunau Power Test Circuit.

[19] AEG.TELEFUNKEN.BBC—SIEMENS (1970) Cooperation on the Transmission of Electrical Energy by High-Voltage Direct Current (HVDC) September 1970, Bulletin No. 6.

[20] ESR (2015) Physical Description of the Electricity Distribution Network (DPN).

[21] Lilien, J. (2000) Transport and Distribution of Electrical Energy. Practical Work Manual for the Course, University of Liège.

[22] Bouazza, D. (2021) Industrial Electrical Networks. Course Notes for Master 2 Students in Electrical Networks. PP. 74-115. https://fsa.univ-tiaret.dz/images/doc/COURS/reseauxel.pdf

[23] Legifrance (2003) Relating to the Technical Requirements for the Design and operation of the Connection to the Public Distribution Network of an Electrical Energy Consumption Installation.

[24] French Standard C13-205 (1994) Practical Guide, Determination of Conductor Sections and Choice of Protective Devices. 56 p.

[25] Kundur, P., Klein, M., Rogers, G.J. and Zywno, M.S. (1989) Application of Power System Stabilizers for Enhancement of Overall System Stability. *IEEE Transactions on Power Systems*, **4**, 614-626. https://doi.org/10.1109/59.193836

[26] Thomasset, G. and Wildit, S.G. (2010) Electrotechnics. 4th Edition, Heritage Editions (De Boeck).

[27] Gracia, M. and Pinel, J. (1998) Gas-Filled Spark Gaps for Protection against Disturbances—Protective Components. Engineering Techniques Publishing, Paris.

[28] Yu, Y.N. (1983) Electric Power System Dynamics. Academic Press.

[29] Valentin, G., Fondeur, R., Bouillon, B.J. and Turpain, J.C. (1996) Medium Voltage Substations. https://www.techniques-ingenieur.fr/base-documentaire/energies-th4/reseaux-electriques-de-distribution-publique-42264210/postes-a-moyenne-tension-d4600/technique-des-postes-hta-d4600niv10007.html

[30] Bornard, P. (2016) Electricity Transmission and Interconnection Network: Operation and Regulation. Energy Regulatory Commission, General Description of Electricity Networks.

[31] Azouaou, R. (2005) Lecture Notes on Computer Calculation of Electrical Networks. Thesis, Mouloud Mameri University of Tizi Ouzou, Algeria.

[32] IEC 60186 (1987) International Electrotechnical Commission Standard Relating to Voltage Transformation.

[33] Stott, B. and Alsac, O. (1974) Fast Decoupled Load Flow. *IEEE Transactions on Power Apparatus and Systems*, **93**, 859-869. https://doi.org/10.1109/tpas.1974.293985

[34] IEC 61850 (2005) International Electrotechnical Commission Standard Relating to Interoperability in Terms of Communication between Different Protection Relays.

[35] Nagrath, I.J. and Kotari, D.P. (1983) Modern Power System Analysis. McGraw-Hill.

[36] Barret, J.P., Bernard, P., Mayer, B. and Caseau, P. (1997) Simulation of Electrical Networks. Eyrolles Edition.

[37] Tinney, W. and Hart, C. (1967) Power Flow Solution by Newton's Method. *IEEE Transactions on Power Apparatus and Systems*, **86**, 1449-1460. https://doi.org/10.1109/tpas.1967.291823

[38] Sivagaraju, S., Viswanatha Rao, J. and Giridhar, M. (2008) A Loop Based Load Flow Method for Weakly Meshed Distribution Network. *APEN Journal of Engineering and Applied Sciences*, **3**, 55-59.

[39] Teng, J.H. (2003) A Direct Approach for Distribution System Load Flow Solutions. *IEEE Transactions on Power Delivery*, **18**, 882-887. https://doi.org/10.1109/tpwrd.2003.813818

[40] De Rosenbaum, G. (1973) Transport of Electrical Energy over Very Long Distances

and in Very Large Quantities Using Alternating Current "Considerations on the Inga-Shaba interconnection". Royal Academy of Overseas Sciences. Technical Sciences Class.

[41] Sabonnadière, J.C. and Hadjsaid, N. (2018) From Electrical Networks to "Smart Grids". https://www.encyclopedie-energie.org/wp-content/uploads/2018/09/art073_Nourredine-Hadjsa%C3%AFd_JeanClaude-Sabonnadier_reseaux-electriques-Smartgrids.pdf

[42] Escané, P. and Escané, J.M. (2022) Linear Electrical Networks with Distributed Constants. https://www.techniques-ingenieur.fr/base-documentaire/energies-th4/reseaux-electriques-lineaires-42258210/reseaux-electriques-lineaires-a-constantes-reparties-d1100/

[43] Energy Regulatory Commission (2016) General Description of Electricity Networks.

[44] Lilien, J. (2000) Transport and Distribution of Electrical Energy. Practical Work Manual Intended for the Course, University of Liège, Belgium.

[45] Didierlaurent, J.F. (2005) Overhead Lines: Support Equipment. Edition, Engineering Techniques D4 424, Paris.

[46] Prévé, C. and Jeannot, R. (1997) Guide to the Design of Industrial Electrical Networks. https://sitelec.org/download_page.php?filename=schneider/guide_conception_reseaux.pdf

[47] Marine, G. (2025) Electrical Overvoltage Definition and Causes. https://izi-by-edf.fr/blog/electricite-surtension-definition-cause/

[48] Karout, W. and Belhadj, S. (2019) Analysis of Electrical Surges and Their Protections. https://biblio.univ-annaba.dz/ingeniorat/wp-content/uploads/2019/10/Karout-Wassila-Belhadj-Soumia.pdf

[49] Wojszczyk, B. and Brandao, M. (2011) High Penetration of Distributed Generation and Its Impact on Electric Grid Performance—Utility Perspective. 2011 *IEEE PES Innovative Smart Grid Technologies*, Perth, 13-16 November 2011, 1-7. https://doi.org/10.1109/isgt-asia.2011.6167146

[50] Sevette, P. (1965) The Economics of Energy in Developing Countries. https://www.persee.fr/doc/reco_0035-2764_1965_num_16_4_407673_t1_0659_0000_001

[51] Enobel (2019) PIRE DO Mongala. Democratic Republic of Congo, DRC 182081 T.

[52] Youssouf, B. (2021) High Voltage Technology. https://elearning.esgee-oran.dz/pluginfile.php/16193/mod_page/content/68/Cours_THT_BRAHAMI.Y.pdf

[53] Willis, H.L. and Scott, W.E. (2000) Distributed Power Generation, Planning and Evaluation. Marcel Dekker.

[54] Maudit, A. (1919) Electrical Installations (Chapter: Transient Phenomena and Applications). Ed Dunod.

[55] Sabonnadière, J.C. and Nouredine, H. (2007) Electrical Lines and Networks 1: Energy Lines. Hermes Lavoisier, 20 p.

[56] Carrive, P. (1991) Distribution Networks—Structure and Planning, Volume D4210, Engineering Techniques Collection. https://www.techniques-ingenieur.fr/base-documentaire/archives-th12/archives-reseaux-et-applications-tiadc/archive-1/reseaux-de-distribution-d4210/planification-des-reseaux-de-distribution-d4210niv10004.html

[57] Kersting, W.H. (2012) Distribution System Modeling and Analysis. CRC Press.

[58] He, Y.J. (2015) Optimization of the Voltage Plan of a Distribution Network Using Distributed Generation. https://theses.hal.science/tel-01219327/file/GLADKIKH_2015_archivage.pdf#:~:text=HAL%20is%20a%20multi%2Ddisciplinary%20open%20access%20archive,ou%20%C3%A9trangers%2C%20des%20laboratoires%20publics%20ou%20priv%C3%A9s